LES for modelling the urban environment

Ian P Castro & Z-T Xie

School of Engineering Sciences, University of Southampton, Southampton, SO17 1BJ, UK

i.castro@soton.ac.uk

1 Introduction

For many obvious reasons there is increasing interest in being able to predict flow and pollutant dispersion within urban environments, particularly regions like city centres. Current meteorological codes used to compute weather systems do not have grid sizes much below O(10) km in the horizontal, with perhaps a few points vertically within the atmospheric boundary layer. They are usually also not designed to be able to cope with high topological gradients (ground slopes). For these reasons, among others, very different computational approaches are required for computing flows at scales down to O(1) m, say, and in regions containing very many (usually) sharp-edged buildings. Such areas might have domain sizes of hundreds of meters and have been termed 'the street scale' region (see [1], where it was also suggested that the entire city domain be termed the 'city scale', with 'neighbourhood scale' for regions in between street scale and city scale). There are increasing numbers of full-scale field campaigns in which velocities and concentrations are measured within urban areas (see [13] for a recent example). Whilst these can be extremely useful, they are inevitably limited in terms of the data obtained and the extent to which conclusions about the physical processes can be unambiguously made. Computational approaches arguably have much greater potential in this regard. However, even the most optimistic projections of available computer power over the next few decades suggest that it is very unlikely that a single computational tool could be created for accurate modelling of such street scale regions simultaneously with complete city scale regions, and beyond to mesoscale domains.

One of the UK Natural Environment Research Council's collaborative centres is the National Centre for Atmospheric Science, whose Weather Directorate's strategy includes the objective of developing tools to allow prediction of flow, turbulence and dispersion within urban environments. In 2004 a possible route towards this goal was identified, having two major constituent parts. It was recognised that (i) standard RANS modelling was likely to be inadequate for street-scale flows, (ii) LES techniques represented perhaps the lowest-order approach which has any hope of capturing those genuine unsteady features in such flows which crucially affect dispersion processes, and (iii) modern commercially available *engineering-type* codes have much more sophisticated numerics and meshing strategies than even a decade ago, and have sophisticated pre- and post-processor tools. So rather than developing new versions of *meteorological-type* codes, the first part of the approach was to validate the use of commercially available codes – FLUENT, STAR-CD or CFX – for, initially, neutrally stable street scale flows, using available experimental data and (more limited) DNS data for boundary layer flows over very rough surfaces comprising arrays of cuboid obstacles. The second strand was to develop appropriate ways of using the output from meteorological codes (like the UK Met Office's Unified Model) to provide dynamic boundary conditions for the street scale computation.

This paper presents some of our most important conclusions from the work undertaken thus far in the context of the first of these two strands. We have found (i) that, perhaps surprisingly at first sight, LES for flows over such complex surfaces is in fact less technically demanding than for smooth surfaces at similar Reynolds numbers (the flow dynamics are dominated by obstacle-scale motions rather than thin boundary layers), (ii) that a highly efficient filter technique can be used to provide appropriate turbulence inlet conditions, and (iii) that the overall approach can yield flow and concentration results in good agreement with experimental data. §2 outlines the basic numerical methods used and shows some typical validation results whilst §3 presents further results for a generic urban-type surface. The final section, §4, presents some results obtained for a real case – an extensive 'street-scale' region of central London for which flow, turbulence and scalar concentration data are available from both the site itself and a wind tunnel model.

2 Techniques and validation

In view of space limitations, only a brief description of the numerical methods is given here; more extensive details can be found in [21], hereafter denoted by XC.

The filtered continuity and Navier-Stokes equations are written as follows,

$$\frac{\partial u_i}{\partial x_i} = 0$$

$$\frac{\partial u_i}{\partial t} + \frac{\partial u_i u_j}{\partial x_j} = -\frac{1}{\rho}\left(\frac{\partial p}{\partial x_i} + \delta_{i1}\frac{\partial \langle P\rangle}{\partial x_1}\right) + \frac{\partial}{\partial x_j}\left(\tau_{ij} + \nu\frac{\partial u_i}{\partial x_j}\right) . \quad (1)$$

The dynamical quantities, u_i, p are resolved-scale (filtered) velocity and pressure respectively and τ_{ij} is the subgrid-scale (SGS) Reynolds stress. δ_{i1} is the Kronecker-delta and ν is the kinematic viscosity. $\partial\langle P\rangle/\partial x_1$ is the driving force, a constant streamwise pressure gradient. For the sub-grid stresses the classical Smagorinsky SGS model, or a very similar model discussed in [24], was used and in the near-wall region the Lilley damping function was also applied. This reduces the filter width within the viscosity-affected region so that energy-carrying eddy sizes scale appropriately.

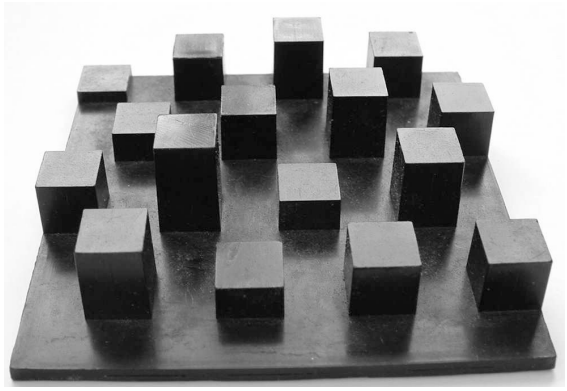

Figure 1: *Random height roughness array.*

For complex geometries like those in view here, where multiple separation and attachment processes occur, it is impossible to satisfy the common criterion that the distance between the centroid of the first cell in (local) wall units should be of order unity. However, one of the conclusions of our earlier work is that this is, in fact, not necessary. A typical urban-like surface is shown in figure 1 and it turns out that the drag of such surfaces is almost entirely form drag. The turbulent motions generated at scales of O(h), where h is an appropriate dimension of the typical roughness element, are dominant and it is not necessary to resolve fine details of the individual (and very thin) boundary layers on each of the element surfaces. This means, too, that applying standard wall-law conditions (i.e. log-law parameters for the near-wall points) is quite adequate, even though it is fundamentally inappropriate as there are probably very few, if any, regions on the element surfaces where log-law conditions actually apply in practice.

However, it *is* necessary to resolve each of the roughness elements adequately (see also [20, 11, 12]). XC showed that, in the context of a staggered array of cubical elements (arranged as in fig.1 but with each element a cube of height h), structured meshes, uniform in the region of the roughness elements, with around 15-20 nodes over the height of the cube, yielded mean velocity, surface pressure and turbulence data in good agreement with both experimental data and fully-resolved DNS results [3]. We will show below results of computations for the surface shown in figure 1. A computational domain embodying four of the complete units shown in figure 1 was used, in a 2 x 2 arrangement, with the oncoming flow normal to the elements at the top of the view and periodic conditions applied in the streamwise and lateral directions. Note that each of the four units contains 16 elements, whose heights are distributed normally, with a standard deviation of $0.3h$ where h is the average height of the elements. Experimental data are available for this surface from a comprehensive programme of measurements in a wind tunnel boundary layer developing over the surface (with $h = 10$ mm, [2]). Stress free conditions were applied at the top of the domain, which was at $z/h = 10$, where $z = 0$ is the bottom surface. The computations thus represented fully-developed flow in a half-channel – practically easier to compute than a boundary layer flow and common in LES computations of atmospheric boundary layers (e.g. [16, 19]). If the emphasis is on the roughness sub-layer and canopy regions, channel computations

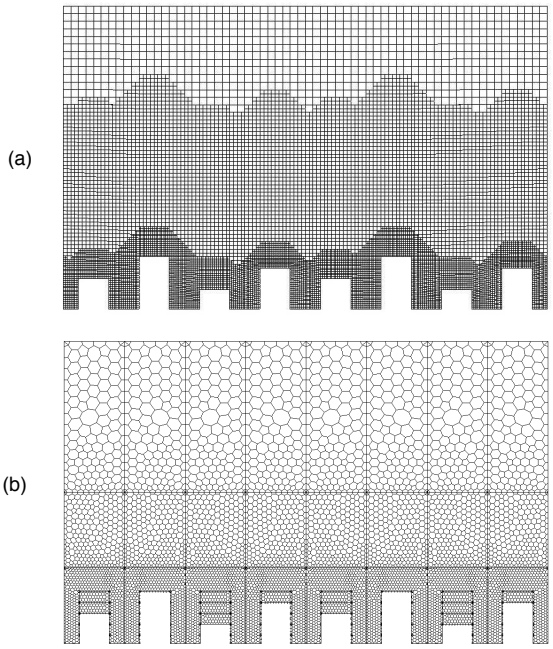

Figure 2: Side-views of meshes, from a vertical-transverse cut across the tallest element. (a): hexahedral mesh; (b): polyhedral mesh.

with a domain height not too dissimilar to the experimental boundary layer thickness are quite adequate (see also XC).

For time-stepping, a second-order backward implicit scheme was used with a time step of $0.002T$ ($T = h/u_\tau$ where u_τ is the usual friction velocity appropriate for the entire surface – related therefore to the total surface drag). The initial duration of most of the runs was $150T$, whereas the subsequent averaging duration for all the statistics was approximately $300T$. [3] found that for their array of uniform cubes, with a spanwise domain size of $8h$, the converging flow contained quite strong, large-scale structures having longitudinal vorticity. These rolls, typically having a spanwise wavelength of about $4h$, gave rise to significant dispersive stresses (i.e. stresses which arise from spatial inhomogeneities in the time-averaged fields) and adequate time-averaging was necessary to resolve statistics unequivocally (i.e. to reduce these dispersive stresses to zero above the near-wall region). They found that an averaging time of about $400T$ was necessary. For the present surface, there was little evidence of such rolls, partly no doubt because of the more random nature of the surface but also perhaps because the spanwise domain was limited to two repeating units (compared with four in [3] and see also [5, 6]). So the $300T$ averaging time in the present case was quite sufficient for obtaining converged statistics.

For spatial differencing we used either a deferred correction second-order central scheme (for the hexahedral mesh run with FLUENTv.6) or the second-order monotone advection and reconstruction scheme (MARS, for the polyhedral mesh used with STAR-CD4). The former employed 2.3 million cells, with $16 \times 16 \times 16$ per $h \times h \times h$ in the near-wall region, and the latter had 1.3 million cells with $13 \times 13 \times 13$ per $h \times h \times h$ in the near-wall region. It must be emphasised that provided discretisation of all terms

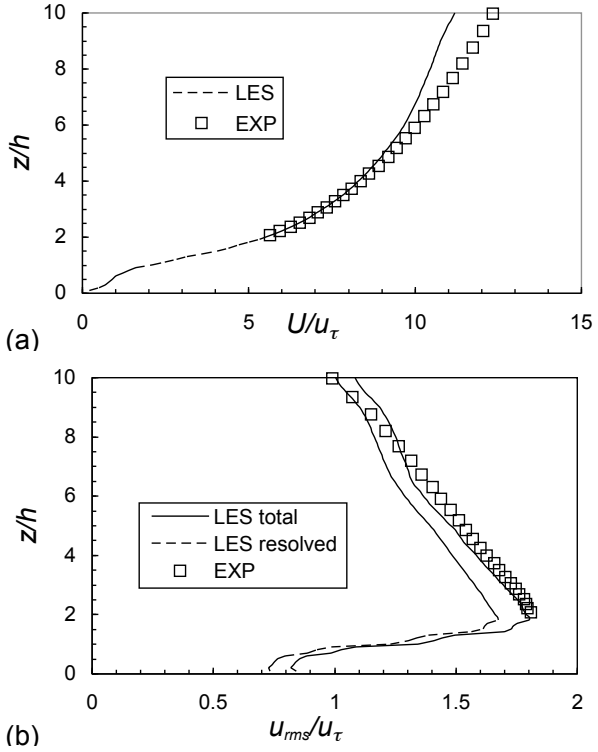

Figure 3: Vertical profiles of spatially averaged mean velocity (a), axial velocity r.m.s. (b).

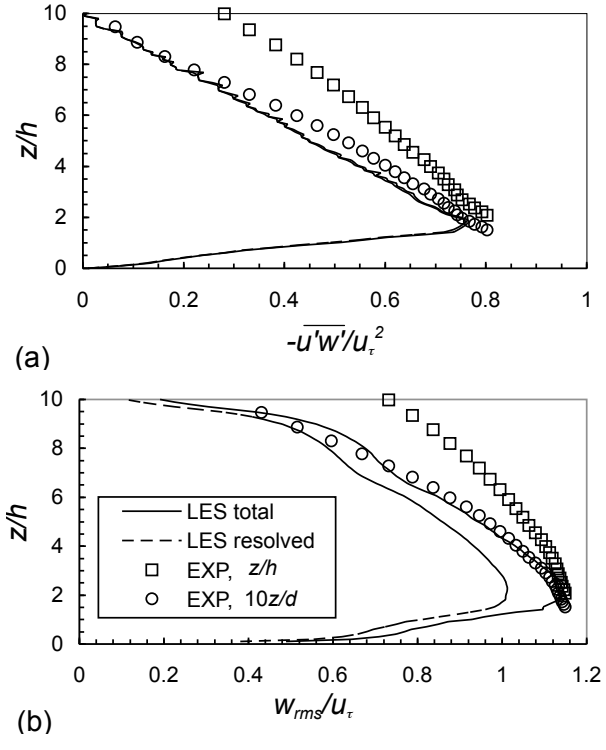

Figure 4: Vertical profiles of spatially averaged vertical velocity r.m.s. (a) and Reynolds shear stress (b). Open circles refer to the experimental data but have the ordinate scaled by boundary layer thickness, $\delta/10$ rather than h.

in Eq.(1) was at least second-order accurate in both space and time, results did not depend perceptibly on the particular LES code employed, nor indeed on the particular mesh chosen provided there was enough resolution in the wall region (as discussed above, with smallest grid sizes no greater than around $0.06h$ near the building edges). It is known that polyhedral meshing is much more flexible than the alternatives for complex geometries and it is also more accurate and less memory consuming than the widely used tetrahedral mesh (see, for example, [17] and note also [4]). Figure 2 shows views of the two meshes used in obtaining the results discussed below.

As an example of the extensive validation process undertaken for arrays of both cubical obstacles and the random-height array shown in figure 1, figures 3 & 4 plot the spatially averaged mean streamwise velocity, velocity r.m.s. and the Reynolds shear stress profiles for the latter case. Periodic conditions were used for inlet and outlet conditions and symmetry at the upper boundary, as discussed earlier. Note that the boundary layer thickness over the wind tunnel array was 137mm, while the depth of the computational domain is 100mm. This causes inevitable differences in the upper region of the domain for the quantities involving the vertical velocity fluctuations (i.e. w_{rms} and $\overline{u'w'}$). Normalising the height by the boundary layer thickness (or domain height) leads to much closer collapse, as shown in figure 4. We emphasise here that although profiles over the entire domain height must clearly depend on the domain height – the latter is essentially a half-channel height – the flow in the roughness sublayer is *not* strongly dependent on domain height. This was demonstrated in [3] and it allows sensible comparisons with the near-surface region of boundary layer flows over the same roughness, provided the boundary layer thickness is not too much smaller than the computational domain height. Notice also that the sub-grid contributions to the r.m.s. velocities are not insignificant; in figure 3b, for example, good agreement with experiment is obtained only once the sub-grid stress component is included. It is worth mentioning the rather subtle point that whilst it is not possible to calculate the sub-grid energy from the sub-grid stress tensor (whose trace is zero), one can approach the matter the other way around and *estimate* the sub-grid energy *posthoc* using the sub-grid model – which is supposed to represent the unresolved portion of the energy spectrum. This is what was done to deduce the additional contributions providing the (estimated) total stresses and energy in the figure 3, but we emphasise that it is not strictly exact.

Results obtained within the canopy region (for arrays of cubical obstacles) and axial velocity energy spectra (see [21]) confirmed the deduction made from earlier experimental measurements, that at least as far as the large-scale dynamics which determine the surface drag are concerned, flows over surfaces of these kinds are essentially Reynolds number independent. This is a very different situation than obtains for smooth-surface flows which, as is well-known, provide a severe test for LES approaches; unless the grid is fine enough to allow virtually a DNS-type resolution, some kind of matching to a near-surface RANS approach, or equivalent, has to be employed to surmount the difficulty.

Using LES for typical practical situations (as illustrated later) exacerbates the difficulties posed by having to supply appropriate boundary conditions.

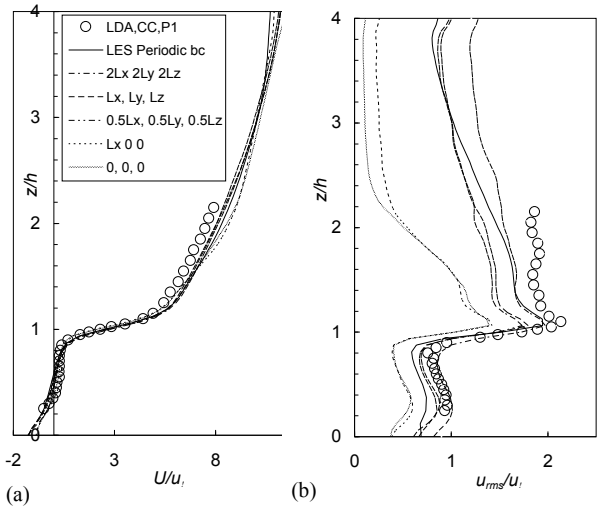

Figure 5: Influence of integral length scale on mean velocity and turbulence at a typical location though a staggered array of cubes. The domain was $16h$ in length and $4h \times 4h$ in cross-section.

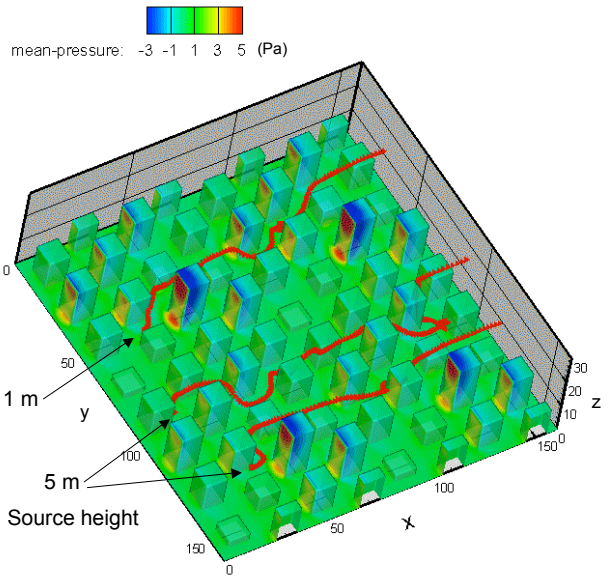

Figure 6: Surface static pressure contours for the array shown in figure 1.

Periodic conditions (in the axial direction) are not appropriate for spatially developing flows and, even if the upstream flow may be taken as essentially steady, one requires an efficient method of inserting appropriate small-scale turbulence at the upstream boundary at each time step. A number of methodologies have been developed to achieve this, including 'modified periodic' methods (e.g. [15]), techniques based on proper orthogonal decomposition [10, 8, 18], and synthetic turbulence generation, usually based on filtering methods (e.g. [14]). Many of these are quite expensive in terms of the overheads in computing time needed just to provide inlet conditions.

We have developed a very efficient and fully three-dimensional version of a filter method [22]. It involves supplying appropriately chosen vertical profiles

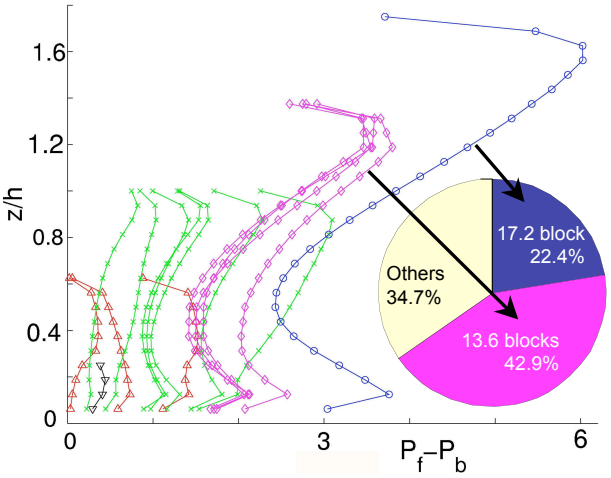

Figure 7: Normalised profiles of laterally integrated pressure difference between front and back faces of the elements.

of Reynolds stresses and integral length scales and, in tests using classical turbulent channel flows, was shown not only to be very much more time-efficient than the nearest equivalent previously published [14] but also more efficient in terms of generating fully developed channel turbulence in as short an axial fetch as possible. The computational efficiency arises specifically through assuming an exponential form for the spatial correlation coefficients, so that the new fluctuating velocity field at each time step can be efficiently formed as an appropriate combination of the previous time step's field and a new 2D filtered random field. In fact, at all but the smallest scales, an exponential correlation is rather more physical than alternative forms like the commonly used Gaussian, so the method is also more physically appealing than many alternatives. As an example of results obtained with the method figure 5 shows profiles of axial mean velocity and rms turbulence, compared with experimental data, for the case of a staggered 25% area coverage array of cubes in a channel. The computations used either periodic conditions or the new, efficient filter method for supplying inlet turbulence (with standard zero-gradient conditions at the downstream boundary). Appropriate inflow stress profiles were used, with considerably simplified profiles of integral length scales (L_x, L_y, L_z, for the axial velocity). The results are not very sensitive to the precise values of these scales – changing all three by a factor of two has only marginal effect on the turbulence (fig.5b). However, if they are not specified at all, so that the inlet turbulence has no genuine spatial structure, then the turbulence decays rapidly. Specifying only axial structure *via* an enforced L_x profile (i.e. with no cross-stream structure so that L_y, L_z are both zero, as done in [9]) is also clearly insufficient. With sensible choices, based on experimental data, the turbulence levels are close to those obtained assuming periodic boundary conditions. The full methodology and validation experiments are presented in [22].

3 Further results for a generic surface

A number of interesting features have been identified from the LES results obtained over the generic

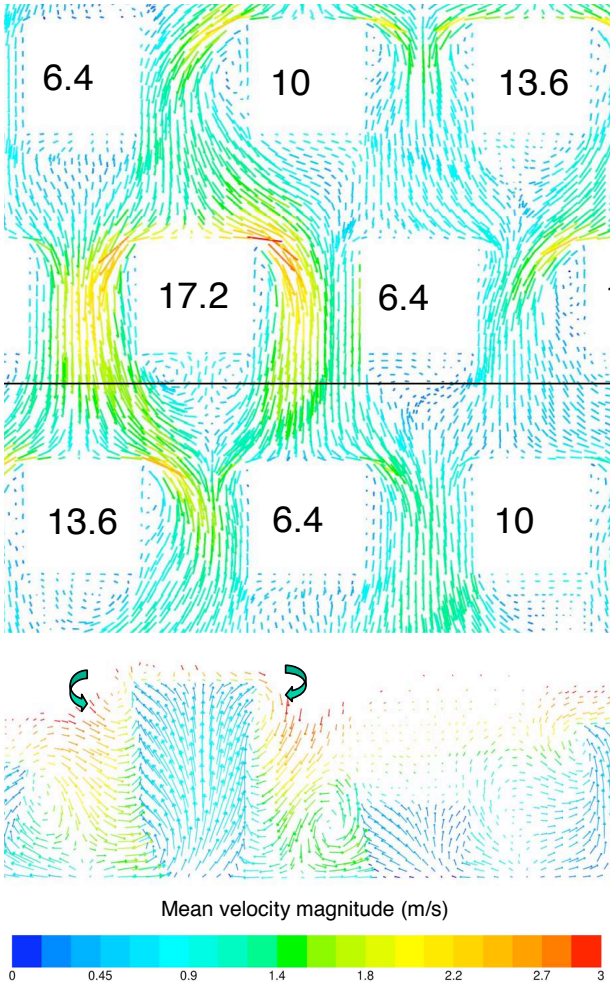

Figure 8: Mean velocity vectors (U, V) at $z = 0.5h$ (top, flow is from top to bottom) and (V, W) on the vertical plane just behind the tallest element (bottom, looking upstream). Only a small section of the full computational domain (four of the complete 16-block units illustrated in fig.1) is shown. Element heights (in mm) are shown in the upper figure.

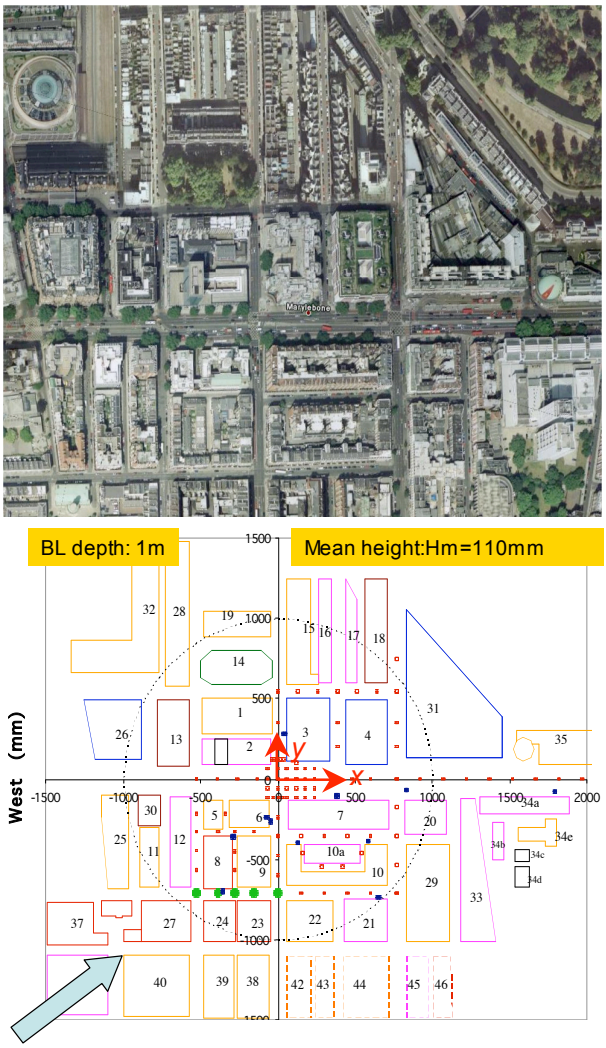

Figure 9: The DAPPLE site in London (top) and a plan of the 1:200 scale wind tunnel model used at the EnFlo laboratory, University of Surrey (bottom). Note the arrow at bottom left, indicating the mean wind direction. Coordinate dimensions are in mm, with roof heights indicated on each building.

urban-type surface represented by the random-height array shown in figure 1. We comment here on two of these. Firstly, LES allows mean and fluctuating information on the element (building) surface pressures to be obtained. Figure 6 shows mean surface pressures and it is immediately clear that the four tallest elements (one in each of the four identical units within the domain, see §2) experience significantly higher surface pressures on the front face than experienced by the other elements. In fact, it turns out that 22.4% of the total surface drag is provided by these tallest elements – very much higher than might be anticipated solely on the basis of their contribution to the total frontal area 'seen' by the flow. Figure 7 shows variations of the front-to-back pressure difference on each of the 16 elements within one unit, which emphasises the relatively large pressures on the tallest element. Although scalar concentration computations and results cannot be discussed in detail here, figure 6 includes an example of such data: time-averaged pathlines for scalar sources located within the roughness canopy. Time-dependent versions of these are also available of course, and this provides a major motivation for using a genuinely unsteady method like LES for such flows – RANS computations cannot in principle (and do not in practice) yield adequate results of this type.

Secondly, it was found that details of the flows around each element are very dependent on element size and location and can be crucially different from those that occur over isolated obstacles. Figure 8 shows mean velocity vectors on a horizontal plane at $z/h = 0.5$ (i.e. in the middle of the canopy region) and on a vertical plane behind the tallest element. Just outboard from the sides of the latter the flow contains a counter-rotating vortex pair, indicated in the bottom view. The sense of the rotation is *opposite* to what would normally occur for an isolated object of the same shape, for which the cross-stream circulations have the same sense as those in a trailing vortex system behind, for example, a delta wing. The reason for the difference can be identified by considering the flows induced by the somewhat lower (but

Figure 10: A section of the polyhedral mesh topology at the ground surface of the computational domain.

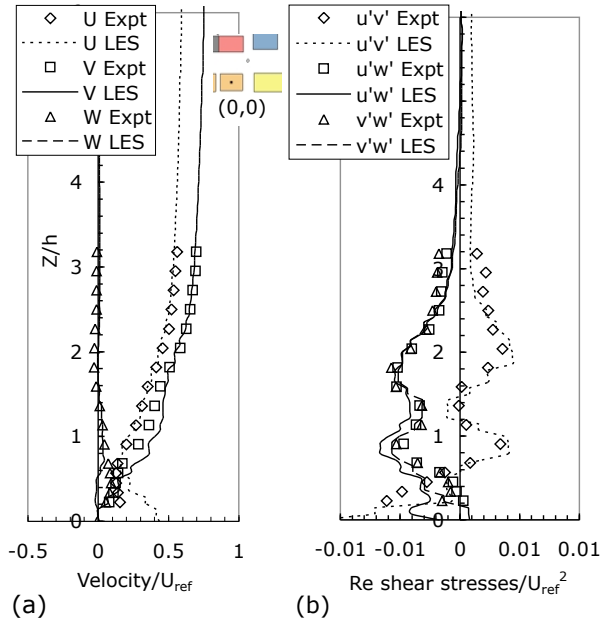

Figure 11: Velocity (a) and turbulence shear stress (b) profiles at the Marylebone Road - Gloucester Place intersection. Experimental data is from LDA measurements.

not equal height) elements located just downstream but, in any case, the results emphasise that even the qualitative behaviour of the flow around a particular object surrounded by others may be entirely different from what might be expected. Detailed studies of the nature of the flow within the canopy region can be found in [5, 23].

4 A practical case

We conclude by presenting results from an LES computation of the flow and dispersion over an area of London surrounding the Marylebone Road. This was a site used for an extensive field campaign, with dispersion from various point sources measured at

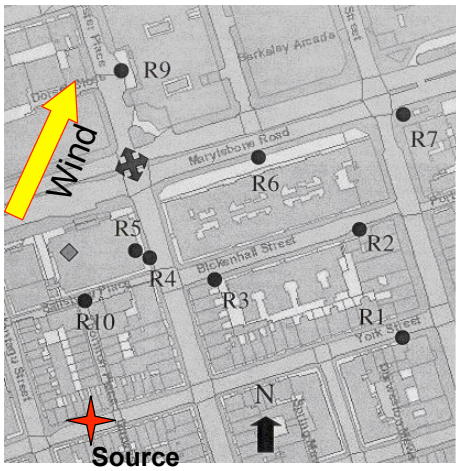

Figure 12: Plan of the field site. The major intersection is shown with a cross at left and the source location is also shown – bottom left. Wind tunnel (and field) receptor locations are numbered R1-10 and shown in the plan, except R8, which is further down Marylebone Road beyond the top right of the view.

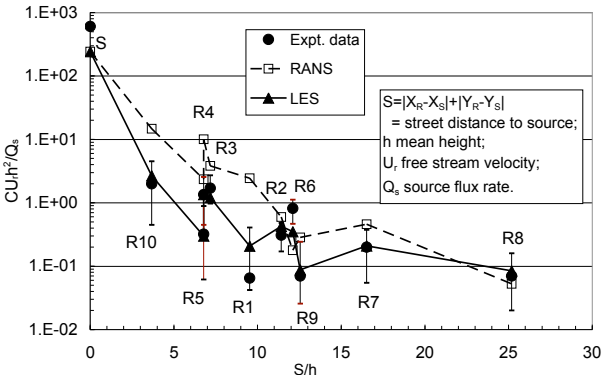

Figure 13: Scalar concentration at $z/h = 0.25$ as function of normalised 'walking distance' (S/h) from the source.

numerous locations under various wind conditions (also measured). A full wind-tunnel model was constructed, allowing a more comprehensive set of data to be obtained for the same source and (simulated) wind conditions. Details can be found at www.dapple.org.uk and a sample publication discussing flow field measurements is [7]. Our computation used a polyhedral mesh of about 1.5 million cells with the smallest ones (adjacent to building surfaces) of around $h/16$ where h is, again, the average building height. The inlet turbulence generation scheme described earlier was used, with symmetric conditions at the lateral boundaries and a stress-free boundary at the top ($z = 10h$). No 'tweaking' of the inlet turbulence profiles was done; we simply employed profiles appropriate for the simulated atmospheric boundary layer upstream of the wind tunnel model. Figure 9 shows a Google map of the actual site, along with a plan of the wind tunnel model, and figure 10 shows the surface mesh. Because of the much greater detail in the wind tunnel database the computations simulated the wind tunnel situation, using the same Reynolds number and wind direction (shown in figure

9).

Two sets of results are shown – vertical profiles of velocity and turbulence at the intersection of Marylebone Road and Gloucester Place, figure 11, and the mean scalar concentration at pedestrian height, figure 13, arising at various locations (shown in figure 12) downwind of a steady source positioned at pedestrian height ($0.07h$, also identified in figure 12). Note first, from figure 11, that there is encouragingly good agreement between experiment and computations for all components of mean velocity and Reynolds stresses. Similar agreement was evident elsewhere in the domain. One of the major motivations for the DAPPLE programme was to acquire scalar concentration data for known meteorological conditions, to allow testing of modelling approaches. So the crucial question in the present context is whether LES yields adequate concentration data. Figure 13, which includes results from corresponding RANS computations, demonstrates that it does. Indeed, it is perhaps remarkable that the time-averaged (normalised) concentrations agree so well with measured values over nearly four orders of magnitude. Note particularly that RANS approaches do not yield such good agreement – there can be differences as great as an order of magnitude at particular locations. Careful scrutiny of all the data showed that this was partly because RANS does not capture the detailed unsteady nature of the flow within the canopy, which is crucial in determining the dispersion processes.

It is concluded that appropriately designed LES approaches have great potential for modelling environmental flows, particularly perhaps those in urban environments. Whilst space has not permitted a discussion of how these street-scale computations can be driven by large-scale fluctuations arising from mesoscale processes, we have already implemented a scheme allowing such fluctuations to drive the input turbulence formulation. There is also, it seems, great promise for this important aspect of the overall approach.

5 Acknowledgements

Thanks are due to the UK Natural Environment Research Council, who funded much of the work summarised in this paper through NCAS grants DST/26/39 and RH/H12/38. Computations were performed on the university of Southampton's IRIDIS system.

Bibliography

[1] Britter R.E. & Hanna S.R., Flow and dispersion in urban areas, *Ann. Rev. Fluid Mech.* **35**, 469-496, 2003.

[2] Cheng H. & Castro I.P., Near wall flow over urban-like roughness, *Boundary-Layer Meteorol.* **104**, 229–259, 2002.

[3] Coceal O., Thomas T.G., Castro I.P. & Belcher S.E., Mean flow and turbulence statistics over groups of urban-like cubical obstacles, *Boundary Layer Meteorol.*, **121**, 491–519, 2006.

[4] Choudhury D, Kim S.E., Makarov B.P. & Carey C., Improved numerical methods for CFD solutions on unstructured meshes, *ERCOFTAC bulletin* **62**, 13–18, 2004.

[5] Coceal O., Thomas T.G. & Belcher S.E., Spatial variablity of flow statistics within regular building arrays, *Boundary Layer Meteorol.*, 2007a.

[6] Coceal O., Dobre, A., Thomas T.G. & Belcher S.E., Structure of turbulent flow over regular arrays of cubical roughness, *J. Fluid Mech.*, **589**, 375–409, 2007b.

[7] Dobre A., Arnold S.J., Smalley R.J., Boddy J.W.D., Barlow J.F., Tomlin A.S. & Belcher S.E., Flow field measurements in the proximity of an urban intersection in London, UK. *Atmos. Environ. 39*, 4647–4657, 2005.

[8] Druault P., Lardeau S., Bonnet J.-P., Coiffet F., Delville J., Lamballais E., Largeau J.F. & Perret L., Generation of three-Dimensional turbulent inlet conditions for large-eddy simulation, *AIAA J.* **42**(3) 447-456, 2004.

[9] Hanna S.R., Tehranian S., Carissimo B., Macdonald R.W. & Lohner R., Comparisons of model simulations with observations of mean flow and turbulence within simple obstacle arrays, *Atmos. Environ.* **36**, 5067-5079, 2002.

[10] Johansson P.S. & Andersson H.I., Generation of inflow data for inhomogeneous turbulence, *Theor. and Comput. Fluid Dyn.*, *18*, 371–389, 2004.

[11] Kanda M., Large-Eddy Simulations of the effects of surface geometry of building arrays on turbulent organised structures, *Boundary Layer Meteorol.* **118**. 151–168, 2006.

[12] Kanda M., Moriwaki R. & Kasamatsu F., Large-eddy simulation of turbulent organized structures within and above explicitly resolved cube arrays, *Boundary Layer Meteorol.* **112**, 343-368, 2004.

[13] Kastner-Kline P. & Rotach M.W., Mean flow and turbulence characteristics in an urban roughness sublayer, *Boundary Layer Meteorol.* **111**, 55–84, 2004.

[14] Klein M., Sadiki A. & Janicka J., A digital filter based generation of inflow data for spatially developing direct numerical simulation or large eddy simulation, *J. Comp. Phys.* **186**, 652–665, 2003.

[15] Lund T., Wu. & Squires D., Generation of turbulent inflow data for spatially developing boundary layer simulation, *J. Comp. Phys.*, *140*, 233–258, 1998.

[16] Moeng C.-H., A Large-Eddy Simulation model for the study of planetary boundary layer turbulence, *J. Atmos. Sci.* **41**, 2052–2062, 1984.

[17] Peric M., Flow simulation using control volume of arbitrary polyhedral shape, *ERCOFTAC bulletin* **62**, 25–29, 2004.

[18] Perret L., Delville J., Manceau R. & Bonnet J.P., Generation of turbulent inflow conditions for large eddy simulation from stereoscopic PIV mearurements, *Int. J. Heat Fluid Flow* **27**(4) 576–584, 2006.

[19] Shaw R. H. & Schumann, U., Large Eddy Simulation of turbulent flow above and within a forest, *Boundary Layer Meteorol.* **61**, 47–64, 1992.

[20] Stoesser T., Mathey F., Frohlich J. & Rodi W., LES of flow over multiple cubes. *ERCOFTAC Bulletin* **56**, 2003.

[21] Xie Z.-T. & Castro I.P., LES and RANS for turbulent flow over arrays of wall-mounted cubes, *Flow,Turbulence and Combustion*, **76** (3), 291–312, 2006.

[22] Xie Z.-T. & Castro I.P., Efficient generation of inflow conditions for Large Eddy Simulation of street-scale flows, *Flow,Turbulence and Combustion*, in press, 2008, DOI: 10.1007/s10494-008-9151-5.

[23] Xie Z.-T., Coceal O. & Castro I.P., Large-eddy simulation of flows over random urban-like obstacles, *Bound. Layer Meteorol.*, in press, 2008.

[24] Yoshizawa A., Statistical theory for compressible turbulent shear flows, with the application to subgrid scale modelling, *Phys. Fluids* **29**, 2152– 2164, 2006.